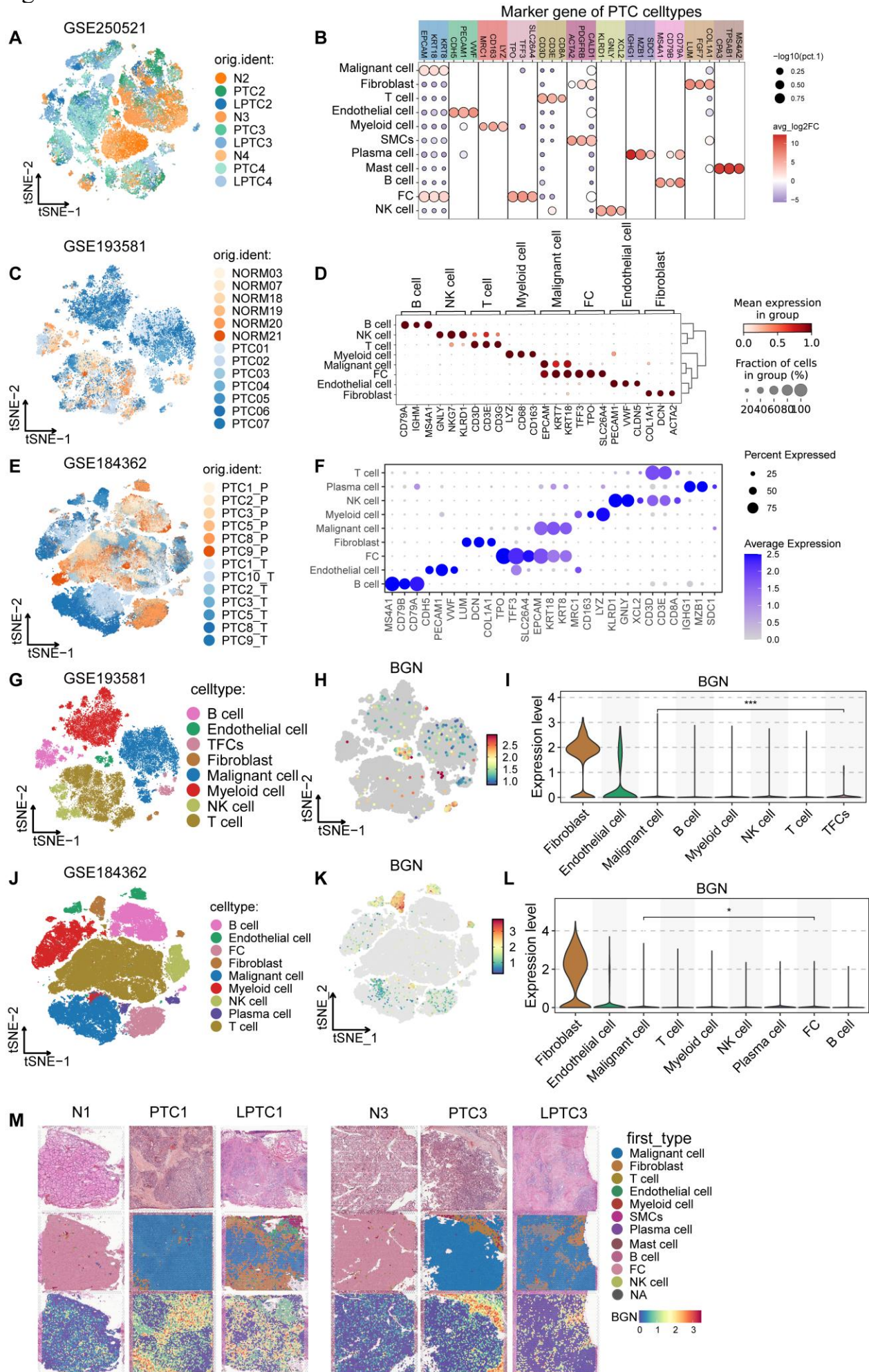
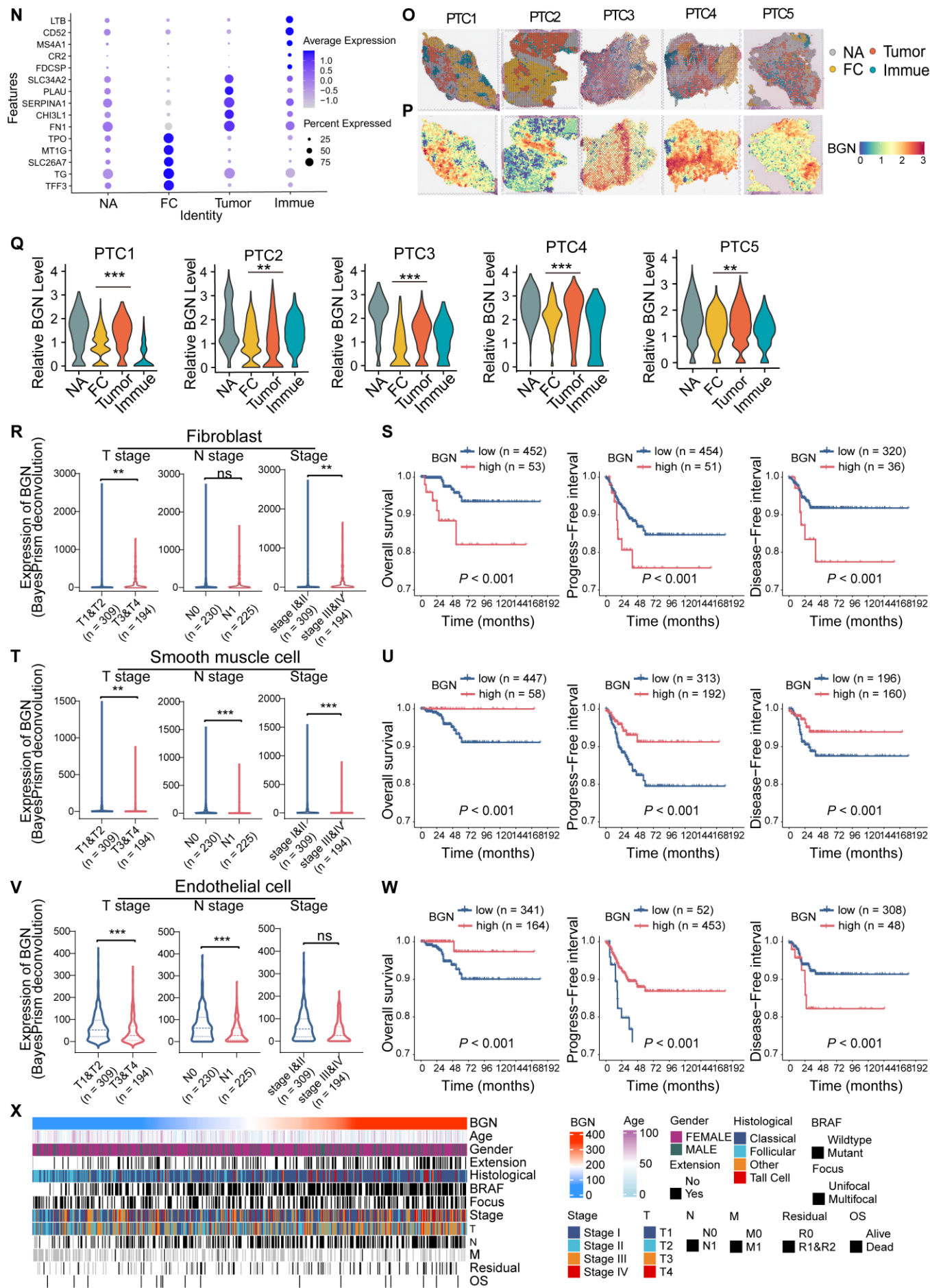


**Enhancer-mediated NR2F2 recruitment activates BGN to  
promote tumor growth and shape tumor microenvironment in  
papillary thyroid cancer**

*Mei Tao, Xianhui Ruan, Jialong Yu, Qiman Dong, Wei Luo, Wei Zhang, Mengran  
Tian, Xiukun Hou, Linfei Hu, Jingzhu Zhao, Dapeng Li, Jie Hao, Songfeng Wei,  
Xiangqian Zheng, Ming Gao*

Figure S1

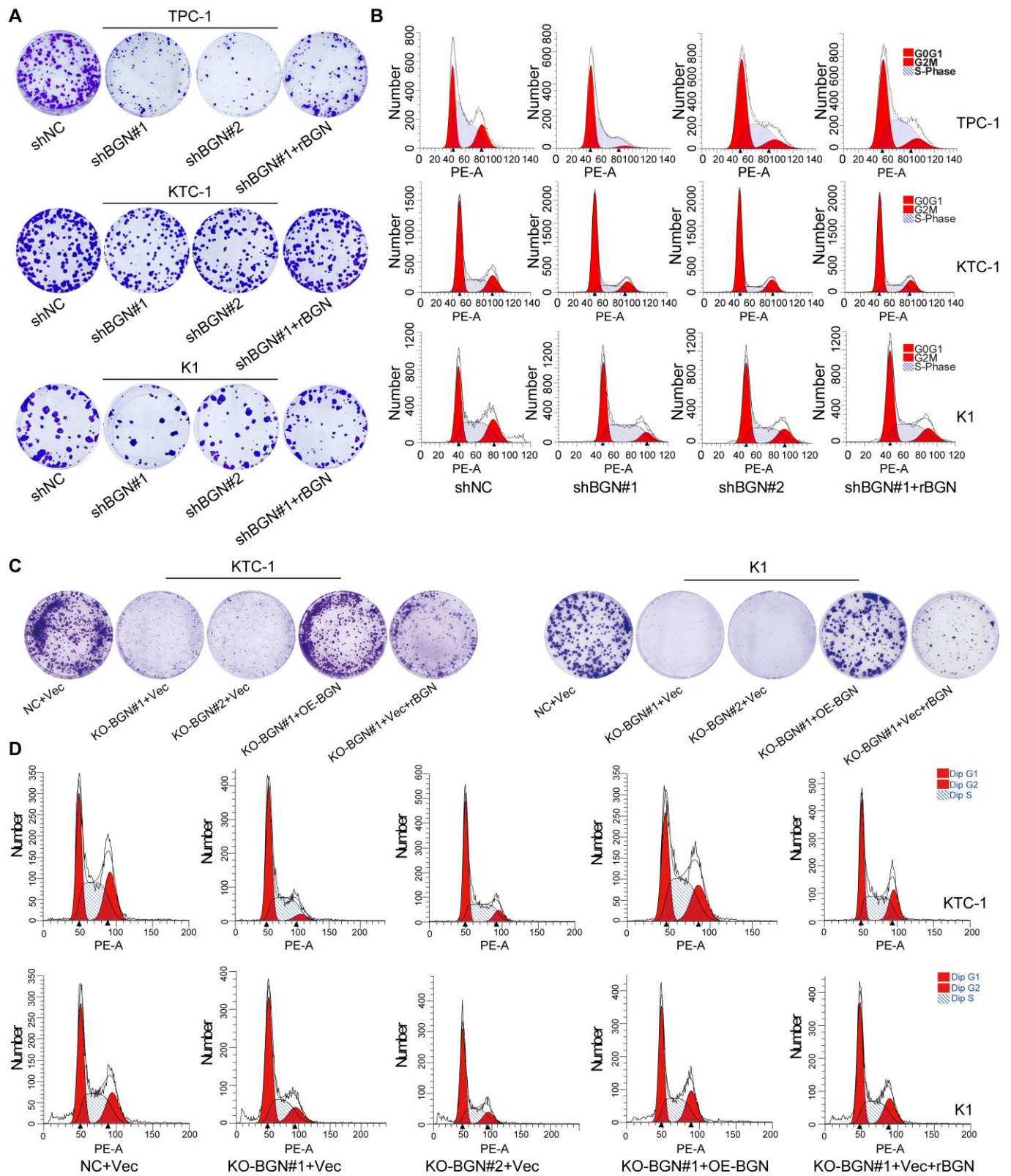




**Figure S1.** (A, C, E) t-SNE plots of scRNA-seq datasets GSE250521 (A), GSE193581 (C), and GSE184362 (E) showing sample distribution. (B, D, F) Dot plots of cell-type-specific marker genes for each dataset. (G, J) t-SNE plots of scRNA-seq datasets GSE193581 (G) and GSE184362 (J) showing cell types distribution. (H, K) BGN expression mapped on t-SNE scatter plots of scRNA-seq datasets GSE193581 (H) and GSE184362 (K). (I- L) Violin plots comparing BGN expression between malignant cells and normal thyroid follicular cells in the scRNA-seq datasets GSE193581 (I) and GSE184362 (L). (M) Spatial distribution of BGN expression in spatial transcriptomics dataset GSE250521. (N-O) Spatial segmentation of normal and tumor regions in five PTC samples using Yan et al.'s framework. (P-Q) Distribution (P) and Violin plots (Q) of BGN expression in tumor vs. normal spots across five sections. (R, T, V) Violin plots showing differences in relative BGN expression levels in fibroblast (R), smooth muscle cell (T), and endothelial cell (V), as determined by BayesPrism deconvolution analysis, among different clinicopathological subgroups. (S, U, W) Kaplan–Meier survival analysis demonstrates that high fibroblast (S), smooth muscle cell (U), and endothelial cell (W) secreted BGN expression, classified by the optimal cutoff from BayesPrism deconvolution analysis, is associated with poorer overall survival (OS), progression-free survival (PFS), and disease-free survival (DFS) in PTC patients. (X) Heatmap illustrating the BGN expression levels and their associations with clinicopathological features in the PTC patient cohort. (\* $p < 0.05$ , \*\* $p < 0.01$ , \*\*\* $p < 0.001$ ).



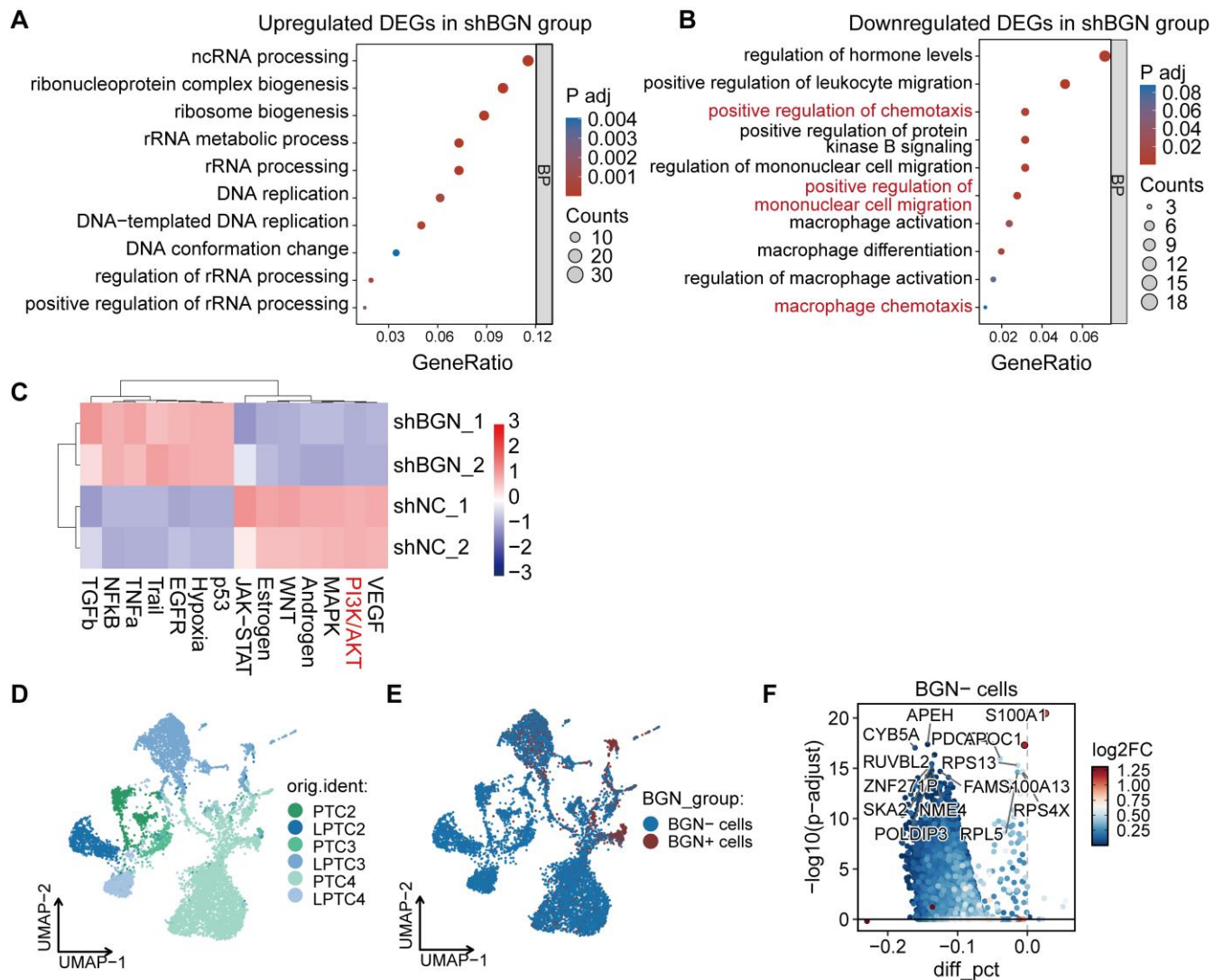
Figure S2



**Figure S2.** (A) Representative images of colony formation assays showing the impact of BGN knockdown or rBGN supplement on the proliferation of TPC-1, KTC-1, and K1 cells. (B) Representative flow cytometry images illustrating changes in cell cycle distribution in TPC-1, KTC-1, and K1 cells following BGN

knockdown or rBGN supplement. **(C)** Representative images of colony formation assays showing the impact of BGN knockout, BGN overexpression or rBGN supplement on the proliferation of KTC-1 and K1 cells. **(D)** Representative flow cytometry images illustrating changes in cell cycle distribution in KTC-1 and K1 cells following BGN knockout, BGN overexpression or rBGN supplement.

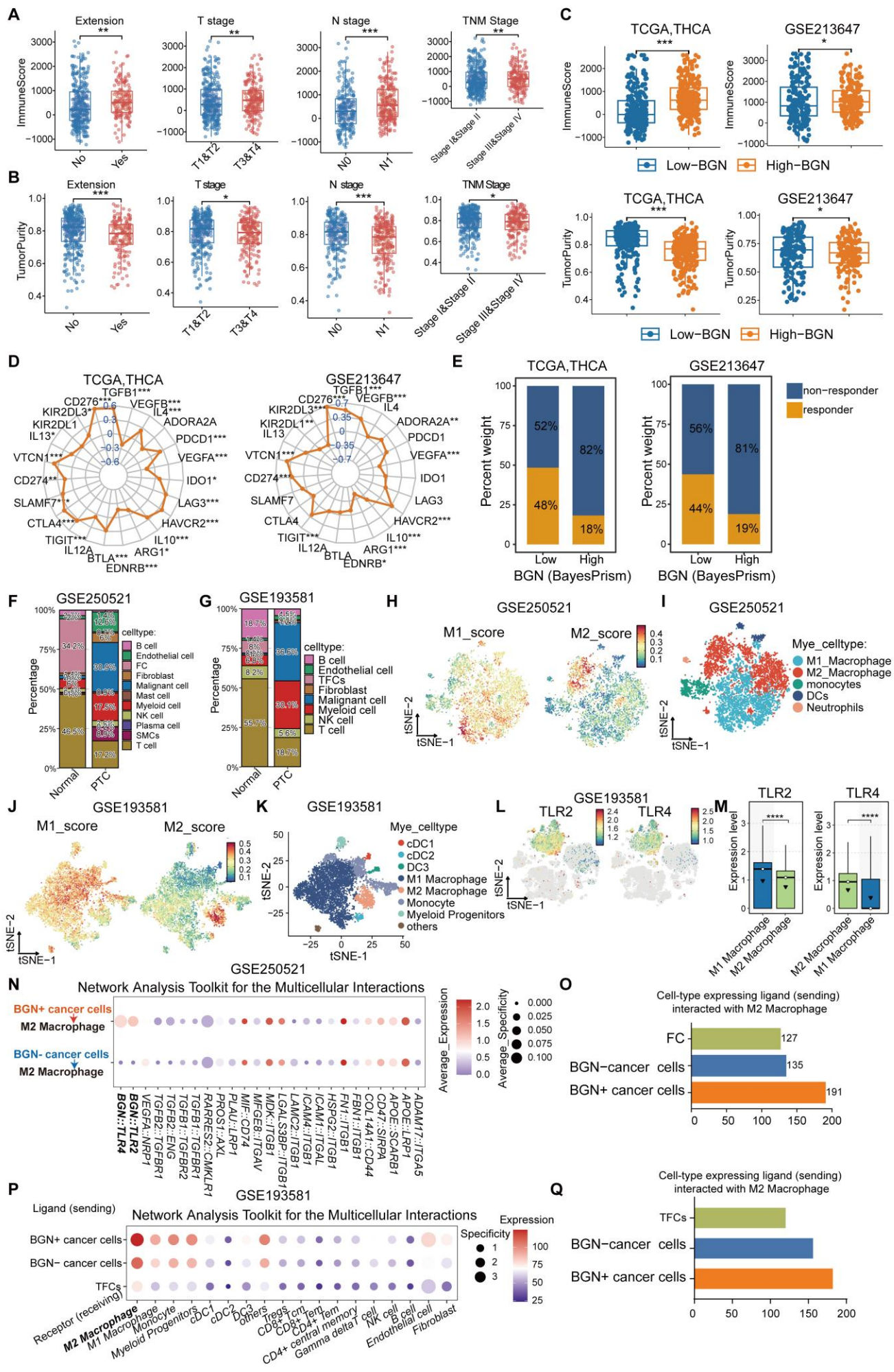
Figure S3



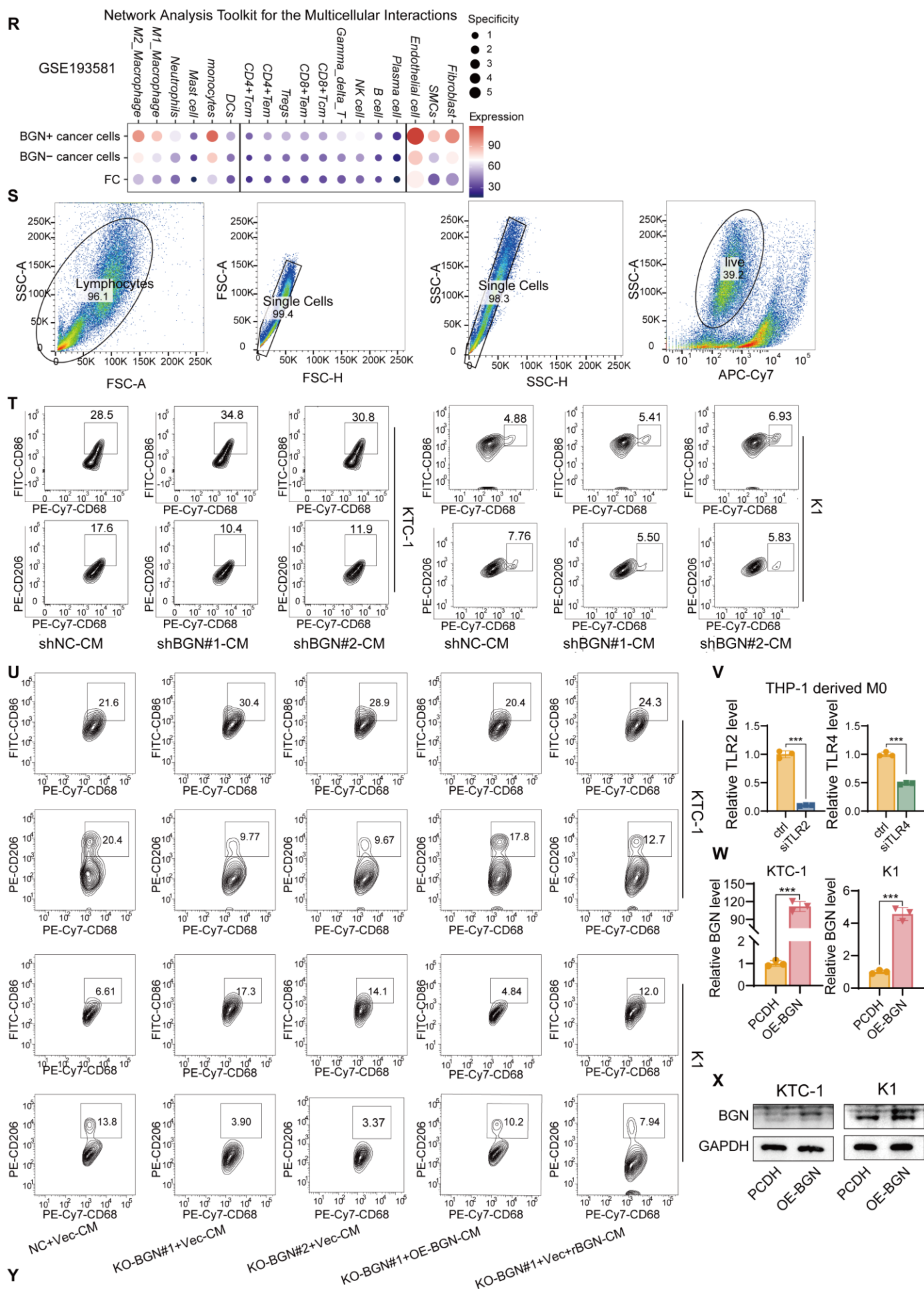
**Figure S3.** (A-B) GO enrichment analysis revealing significantly enriched biological processes among downregulated (A) and upregulated genes (B) in the shBGN group. (C) Heatmap depicting pathway activity in RNA-seq samples analyzed using the “decouplerR” package. (D) UMAP scatter plot of scRNA-seq data from PTC tumor samples (GSE250521) showing the samples distribution. (E) UMAP scatter plot displaying the distribution of BGN<sup>+</sup> and BGN<sup>-</sup> PTC cells across tumor samples. (F) Volcano plot showing different expression genes between BGN<sup>-</sup> and BGN<sup>+</sup> cells.



Figure S4







**Figure S4. (A-B)** Correlation between immune scores (A) or tumor purity (B) and advanced clinical features (extrathyroid invasion, T3/4 stage, N1 stage, TNM III/IV) in the TCGA-THCA dataset. **(C)** Immune score and tumor purity analysis between PTC patients with low and high BGN expression groups based on TCGA and GSE213647 datasets. BayesPrism was applied to obtain tumor cell-specific expression profiles. **(D)** Correlation analysis between BGN expression and immunosuppressive genes. BayesPrism was applied to obtain tumor cell-specific expression profiles. **(E)** Response rate of PTC patients with high BGN expression to immune checkpoint blockade (ICB) therapy. BayesPrism was applied to obtain tumor cell-specific expression profiles. **(F-G)** The cell-type proportions between PTC and normal tissues in the GSE250521 (F) and GSE193581 (G) scRNA-seq datasets. **(H)** t-SNE plot showing the expression of M1 and M2 macrophage scores in myeloid cells from the GSE250521 dataset. **(I)** t-SNE plot illustrating the distribution of myeloid cell subpopulations in the GSE250521 dataset. **(J)** t-SNE plot showing M1 and M2 macrophage scores in myeloid cells from the GSE193581 dataset. **(K)** t-SNE plot displaying the distribution of myeloid cell subpopulations in the GSE193581 dataset. **(L)** t-SNE scatter plot showing the distribution of TLR2 (left) and TLR4 (right) in the GSE193581 single-cell RNA-seq dataset. **(M)** Box plot showing the expression levels of TLR2 and TLR4 in M1 and M2 macrophages from the GSE193581 dataset. **(N)** Bubble plot showing the interaction specificity and strength between BGN+ and BGN- PTC tumor cells, and normal thyroid cells, with microenvironmental cells in the GSE250521 dataset by NATMI. **(O)** Bar graph showing the number of interactions between BGN+ PTC tumor cells, BGN- tumor cells, and normal thyroid cells with M2 macrophages in the GSE250521 dataset. **(P)** Bubble plot depicting the communication strength and specificity between BGN+ and BGN- PTC tumor cells, and normal thyroid cells with microenvironmental cells in the GSE193581 dataset by NATMI. **(Q)** Bar graph showing the number of interactions between BGN+ PTC tumor cells, BGN- tumor cells, and normal thyroid cells with M2 macrophages in the GSE193581 dataset. **(R)** Bubble plot displaying the ligand-receptor interactions between BGN+ tumor cells and M2 macrophages in the GSE193581 dataset by NATMI. **(S)** Gating strategy for macrophage flow

cytometry analysis. **(T)** Representative flow cytometry results of macrophages co-cultured with CM from control and BGN-knockdown groups. **(U)** Representative flow cytometry plots showing M1 and M2 macrophage populations after incubation with CM from the BGN knockout group compared to the control group, and with CM from the BGN overexpression and rBGN supplementation groups compared to the BGN knockout group. **(V)** qRT-PCR validation of TLR2 or TLR4 knockdown efficiency in THP-1-derived macrophages using siRNA. **(W)** qRT-PCR analysis of BGN mRNA levels in KTC-1 and K1 cells with BGN overexpression (OE-BGN) or control (PCDH). **(X)** Western blot analysis of BGN protein levels in KTC-1 and K1 cells with BGN overexpression (OE-BGN) or control (PCDH). **(Y)** Schematic diagram illustrating the experimental design of THP-1-derived macrophages treated with siRNA targeting TLR2 or TLR4, followed by co-culture with CM from BGN-overexpression and control groups. (\* $p < 0.05$ , \*\* $p < 0.01$ , \*\*\* $p < 0.001$ ).



Figure S5

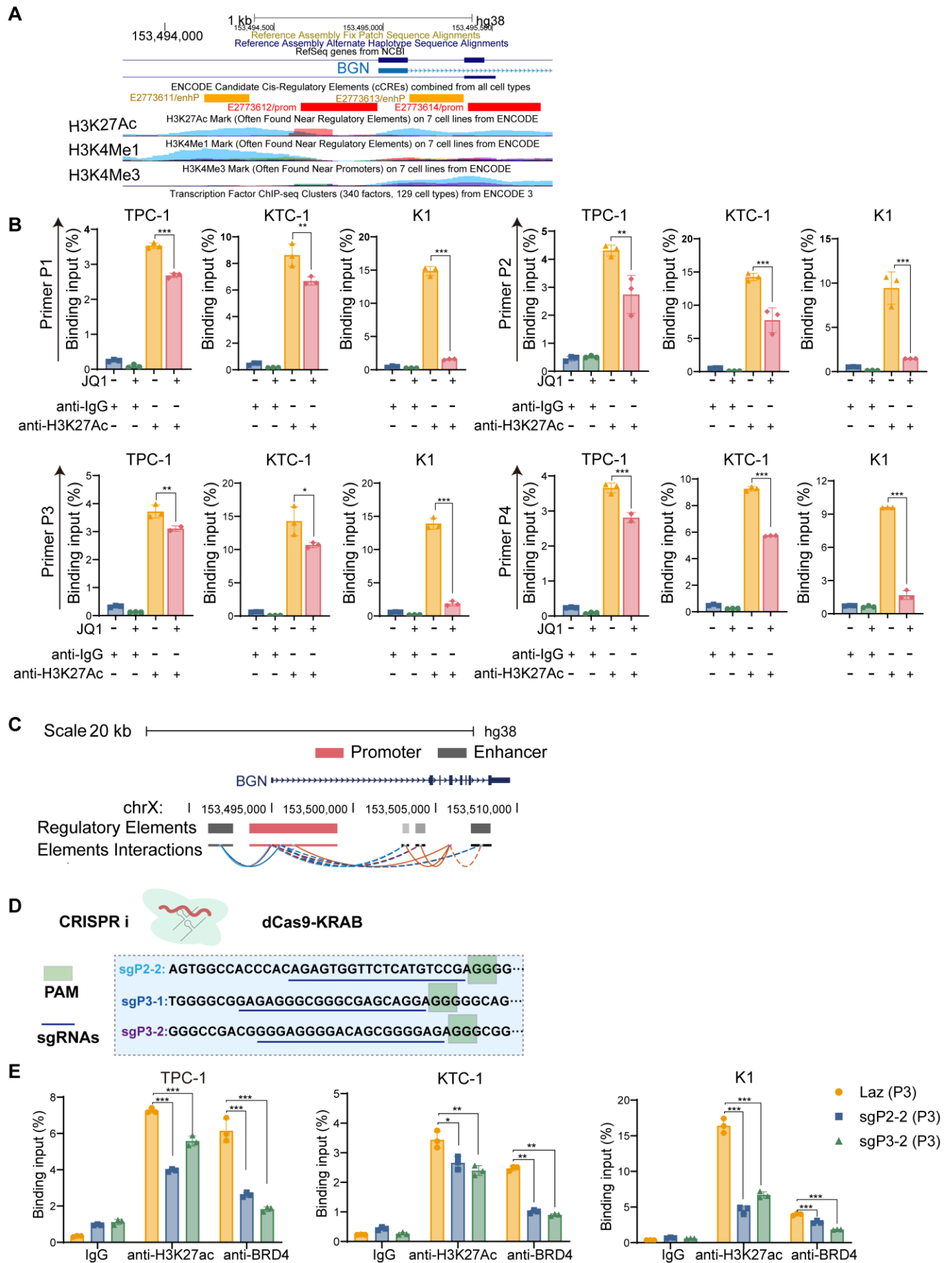


**Figure S5. (A)** H3K27ac, H3K4me1, and H3K4me3 modification profiles at the BGN enhancer and promoter regions based on ENCODE data. **(B)** ChIP-qPCR analysis of H3K27ac modification levels at the

BGN enhancer region after JQ1 treatment. **(C)** GeneHancer database showing that the BGN enhancer regulates the expression of the downstream BGN gene. **(D)** Schematic diagram of CRISPRi targeting the BGN enhancer. **(E)** ChIP-qPCR analysis of H3K27ac and BRD4 levels at the P3 primer region following CRISPRi-mediated knockdown of the BGN enhancer. ( $*p < 0.05$ ,  $**p < 0.01$ ,  $***p < 0.001$ ).

Figure S6

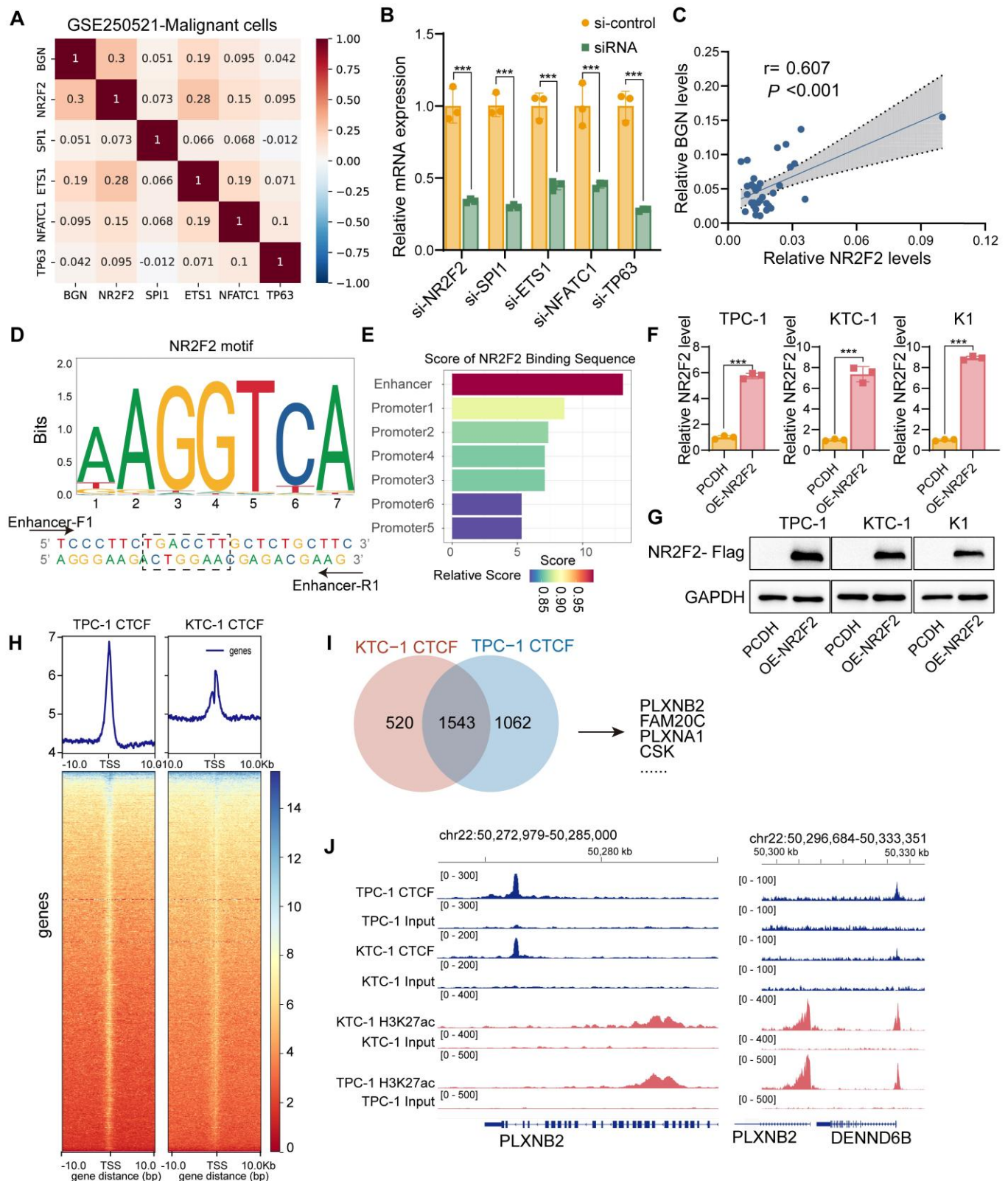
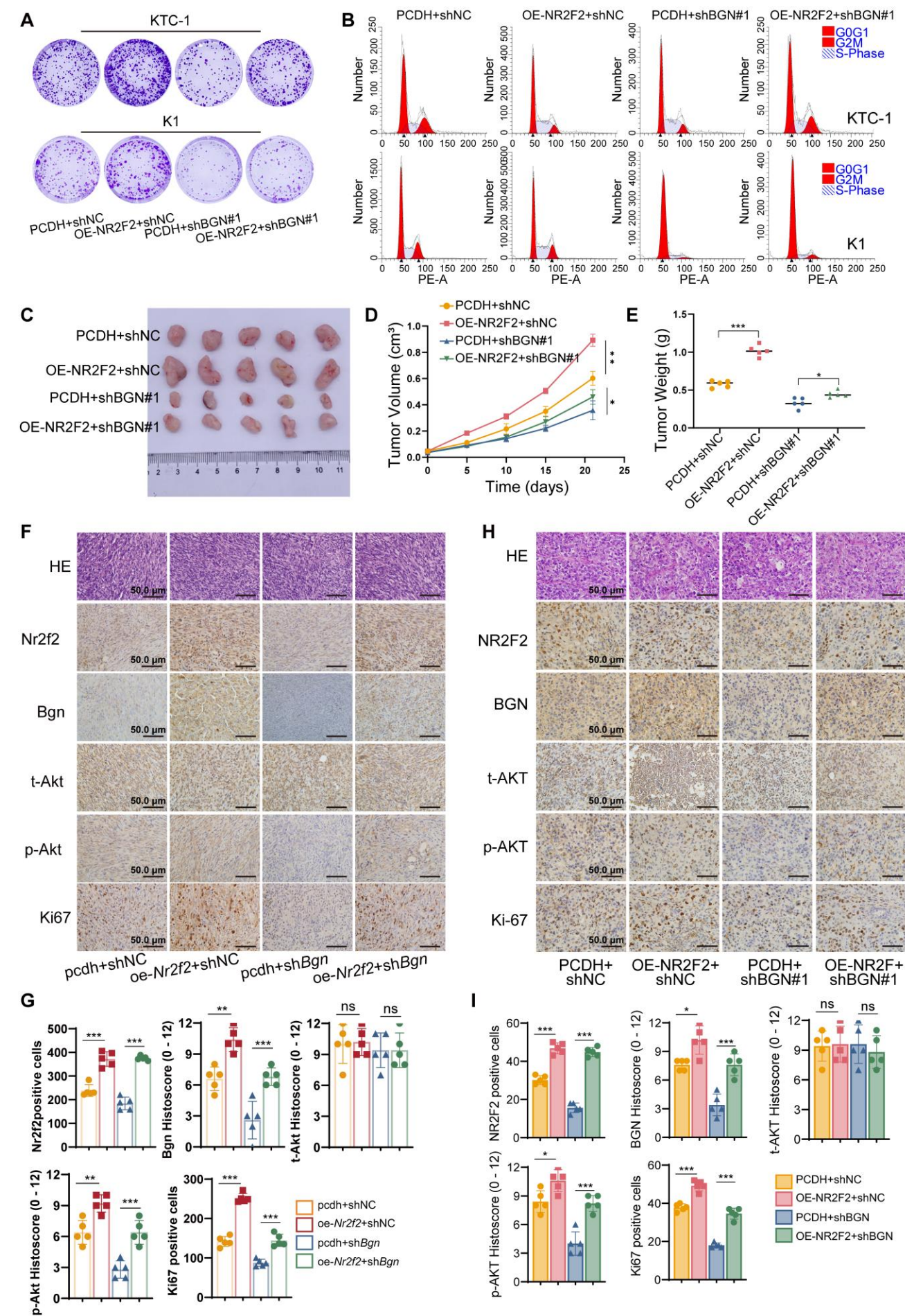


**Figure S6.** (A) Correlation analysis of five transcription factors and BGN expression in malignant PTC cell subpopulations using scRNA-seq data. (B) qRT-PCR validation of knockdown efficiency for NR2F2, SPI1, ETS1, NFATC1, and TP63 using siRNA. (C) Correlation analysis of NR2F2 and BGN mRNA levels in PTC



tissues. **(D)** JASPAR database showing the NR2F2 motif and predicted binding sites at the BGN enhancer. **(E)** JASPAR database predicting binding scores of NR2F2 at the BGN enhancer and promoter. **(F-G)** qRT-PCR (F) and western blot (G) analysis of NR2F2-Flag protein and BGN protein expression in PTC cell lines overexpressing NR2F2. **(H)** The peak plots and Heatmap showing CTCF ChIP-seq enrichment within  $\pm 10$  kb of transcription start sites (TSS) across the genome in TPC-1 and KTC-1 cells. **(I)** The Venn diagram showing the intersection of genes annotated from CTCF peak regions in KTC-1 and TPC-1 cells. **(J)** ChIP-seq tracks for CTCF binding at the PLXNB2 gene promoter and enhancer. (\* $p < 0.05$ , \*\* $p < 0.01$ , \*\*\* $p < 0.001$ ).

Figure S7



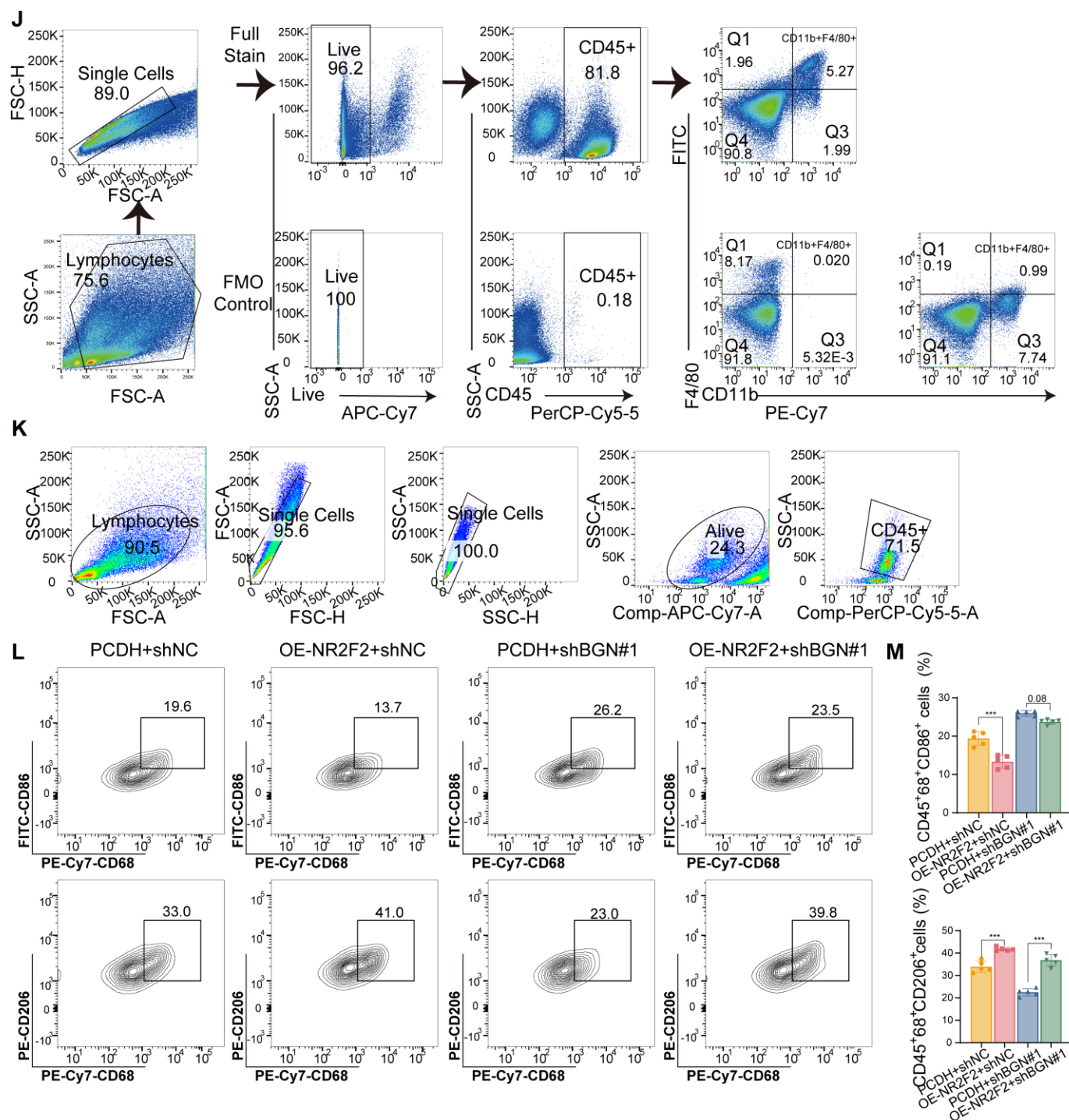


**Figure S7. (A)** Representative images of colony formation assays showing the effects of NR2F2 overexpression and BGN knockdown in KTC-1 and K1 cells. **(B)** Representative flow cytometry images illustrating changes in cell cycle distribution in KTC-1 and K1 cells following the NR2F2 overexpression and BGN knockdown. **(C)** Schematic representation of the nude mouse xenograft model and tumor tissue isolation. **(D)** Tumor growth curves illustrating the effect of the NR2F2-BGN axis on subcutaneous tumor growth in nude mice. **(E)** Tumor weight comparison demonstrating the impact of the NR2F2-BGN axis on



subcutaneous tumor burden. **(F)** Representative immunohistochemical staining images of Nr2f2, Bgn, total Akt, p-Akt, and Ki67 in subcutaneous tumor of C57BL/6J mice treated with PBS liposomes. **(G)** Comparative analysis of immunohistochemical staining scores for Nr2f2, Bgn, total Akt, p-Akt, and Ki67 in subcutaneous tumor of C57BL/6J mice treated with PBS liposomes. **(H)** Representative immunohistochemical staining images of NR2F2, BGN, total AKT, p-AKT, and Ki67 in subcutaneous tumor of nude mice co-injection with THP-1 cells. **(I)** Comparative analysis of immunohistochemical staining scores for NR2F2, BGN, total AKT, p-AKT, and Ki67 in subcutaneous tumor of nude mice co-injection with THP-1 cells. **(J)** Flow cytometry gating strategy for analyzing the proportions of macrophages in subcutaneous tumor of C57BL/6J mice treated with PBS liposomes and Clodronate liposome. **(K)** Flow cytometry gating strategy for analyzing the proportions of macrophages in subcutaneous tumor of nude mice co-injection with THP-1 cells. **(L)** Representative flow cytometry plots showing the proportion of M1 (CD45<sup>+</sup>CD68<sup>+</sup>CD86<sup>+</sup>) and M2 macrophages in different groups. **(M)** Quantification of M1 (CD45<sup>+</sup>CD68<sup>+</sup>CD86<sup>+</sup>) and M2 (CD45<sup>+</sup>CD68<sup>+</sup>CD206<sup>+</sup>) macrophage populations in nude mice subcutaneous tumor tissues. (\* $p < 0.05$ , \*\* $p < 0.01$ , \*\*\* $p < 0.001$ ).

Figure S8

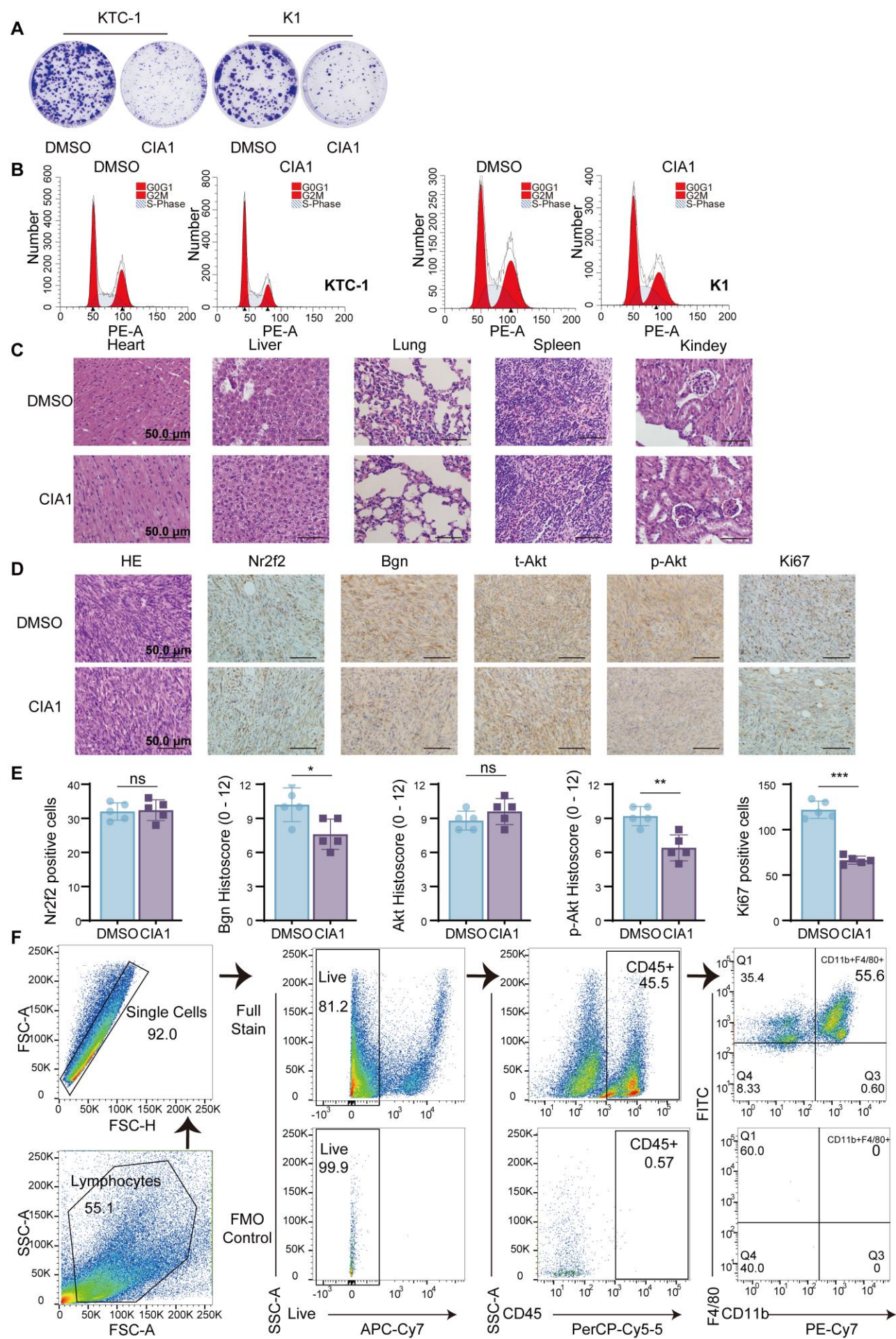


**Figure S8.** (A) Representative images of colony formation assays showing the impact of 5  $\mu$ M CIA1 treatment on KTC-1 and K1 cells proliferation. (B) Representative flow cytometry images illustrating changes in cell cycle distribution in KTC-1 and K1 cells following 5  $\mu$ M CIA1 treatment. (C) HE staining to assess tissue morphology in the heart, liver, and kidneys of mice treated with CIA1 (scale bar: 50  $\mu$ M). (D) Representative IHC staining of tumor tissues from DMSO vs CIA1-treated mice showing Nr2f2, Bgn, Akt, p-Akt, and Ki67 expression (scale bar: 50  $\mu$ M). (E) IHC analysis of positive signal intensity for various tumor markers in DMSO vs CIA1-treated tumors. (F) Gating strategy for macrophage flow cytometry analysis in subcutaneous murine tumor tissues. (\* $p$  < 0.05, \*\* $p$  < 0.01, \*\*\* $p$  < 0.001).



**Table S1.** The samples information for scRNA-seq and spatial transcriptomic datasets in this study.

Sample name	Source	ID	Tissue type	Data type
N2	GSE250521	GSM7980876	Para-tumor	scRNA-seq
N3	GSE250521	GSM7980877	Para-tumor	scRNA-seq
N4	GSE250521	GSM7980878	Para-tumor	scRNA-seq
PTC2	GSE250521	GSM7980879	PTC	scRNA-seq
PTC3	GSE250521	GSM7980880	PTC	scRNA-seq
PTC4	GSE250521	GSM7980881	PTC	scRNA-seq
LPTC2	GSE250521	GSM7980882	LPTC	scRNA-seq
LPTC3	GSE250521	GSM7980883	LPTC	scRNA-seq
LPTC4	GSE250521	GSM7980884	LPTC	scRNA-seq
NORM03	GSE193581	GSM5814577	Para-tumor	scRNA-seq
NORM07	GSE193581	GSM5814582	Para-tumor	scRNA-seq
NORM18	GSE193581	GSM5814593	Para-tumor	scRNA-seq
NORM19	GSE193581	GSM5814594	Para-tumor	scRNA-seq
NORM20	GSE193581	GSM5814595	Para-tumor	scRNA-seq
NORM21	GSE193581	GSM5814596	Para-tumor	scRNA-seq
PTC01	GSE193581	GSM5814574	PTC	scRNA-seq
PTC02	GSE193581	GSM5814575	PTC	scRNA-seq
PTC03	GSE193581	GSM5814576	PTC	scRNA-seq
PTC04	GSE193581	GSM5814578	PTC	scRNA-seq
PTC05	GSE193581	GSM5814579	PTC	scRNA-seq
PTC06	GSE193581	GSM5814580	PTC	scRNA-seq
PTC07	GSE193581	GSM5814581	PTC	scRNA-seq
PTC1_P	GSE184362	GSM5585103	Para-tumor	scRNA-seq
PTC2_P	GSE184362	GSM5585105	Para-tumor	scRNA-seq
PTC3_P	GSE184362	GSM5585108	Para-tumor	scRNA-seq
PTC5_P	GSE184362	GSM5585113	Para-tumor	scRNA-seq
PTC8_P	GSE184362	GSM5585118	Para-tumor	scRNA-seq
PTC9_P	GSE184362	GSM5585120	Para-tumor	scRNA-seq
PTC1_T	GSE184362	GSM5585102	PTC	scRNA-seq
PTC2_T	GSE184362	GSM5585104	PTC	scRNA-seq
PTC3_T	GSE184362	GSM5585107	PTC	scRNA-seq
PTC5_T	GSE184362	GSM5585112	PTC	scRNA-seq
PTC8_T	GSE184362	GSM5585117	PTC	scRNA-seq
PTC9_T	GSE184362	GSM5585119	PTC	scRNA-seq
PTC10_T	GSE184362	GSM5585121	PTC	scRNA-seq
N1	GSE250521	GSM7980860	Para-tumor	spRNA-seq

Sample name	Source	ID	Tissue type	Data type
N2	GSE250521	GSM7980861	Para-tumor	spRNA-seq
N3	GSE250521	GSM7980862	Para-tumor	spRNA-seq
N4	GSE250521	GSM7980863	Para-tumor	spRNA-seq
PTC1	GSE250521	GSM7980864	PTC	spRNA-seq
PTC2	GSE250521	GSM7980865	PTC	spRNA-seq
PTC3	GSE250521	GSM7980866	PTC	spRNA-seq
PTC4	GSE250521	GSM7980867	PTC	spRNA-seq
LPTC1	GSE250521	GSM7980868	LPTC	spRNA-seq
LPTC2	GSE250522	GSM7980869	LPTC	spRNA-seq
LPTC3	GSE250521	GSM7980870	LPTC	spRNA-seq
LPTC4	GSE250521	GSM7980871	LPTC	spRNA-seq
PTC1	HRA003537	HRS493177	PTC	spRNA-seq
PTC2	HRA003537	HRS493178	PTC	spRNA-seq
PTC3	HRA003537	HRS493179	PTC	spRNA-seq
PTC4	HRA003537	HRS493180	PTC	spRNA-seq
PTC5	HRA003537	HRS493181	PTC	spRNA-seq

**Table S2.** Sequences of shRNA, sgRNA and siRNA used in the study.

shRNA / siRNA	5'-3'
shBGN#1	GAAGCTCTACATCTCCAAGAA
shBGN#2	GAACATGAACTGCATCGAGAT
shBGN#3	GCCATTCATGATGAACGATGA
KO-BGN#1-sgRNA	caccGAGAGACACGAGGCGCCACAg
KO-BGN#2-sgRNA	caccGGCCATTCATGATGAACGATg
KO-BGN#3-sgRNA	caccGCCTTGCGGATGCGGTTGTCg
shBgn	CTCCCTGGTAGAACTACGAAT
siTLR2 sense	GGAAGAUAAUGAACACCAATT
siTLR2 anti-sense	UUGGUGUUCAUUAUCUUCCTT
siTLR4 sense	CCAGGUGCAUUUAAAGAAATT
siTLR4 anti-sense	UUUCUUUAAAUGCACCUGGTT
si-NR2F2 sense	GCGAGCTGTTTGTGTTGAATT
si-NR2F2 anti-sense	TTCAACACAAACAGCTCGCTT
si-SPI1 sense	CCUAUGACACGGAUCUAUACC
si-SPI1 anti-sense	UAUAGAUCCGUGUCAUAGGGC
si-ETS1 sense	CCGUGCUGACCUCAAUAAGTT
si-ETS1 anti-sense	CUUAUUGAGGUCAGCACGGTT
si-TP63 sense	GUGUGCUGGUACCUUAUGATT
si-TP63 anti-sense	UCAUAAGGUACCAGCACACTT
si-NFATC1 sense	GGACUCCAAGGUCAUUUUC
si-NFATC1 anti-sense	GAAAAUGACCUUGGAGUCC

**Table S3.** Primer sequences for quantitative real-time PCR.

Primers	5'-3'
BGN-F	GAGACCCTGAATGAACTCCACC
BGN-R	CTCCCGTTCTCGATCATCCTG
ACTB-F	CTCCTTAATGTCACGCACGAT
ACTB-R	CATGTACGTTGCTATCCAGGC
ATF1-F	TCCGACAGCATAGGCTCCTCAC
ATF1-R	CTGTGCCTGGACTTGCCAACTG
MAPK9-F	CGCCCGAAGTCATCCTGGGTAT
MAPK9-R	AGGATACGGTCAGTGCCTTGGA
DDIT4-F	CTTGTGTGCCAACCTGATGC
DDIT4-R	GGAGAGTTGGCGGAGCTAAA
CDKN1A-F	CGATGGAACTTCGACTTTGTCA
CDKN1A-R	GCACAAGGGTACAAGACAGTG
PPP2R5B-F	ACATCCGCAAACAGTGCAAC
PPP2R5B-R	CCCCCAGAAACATCACCTCC
EGFR-F	AGACATGGACGACGTGGTGGAT
EGFR-R	GGAGGTTGAGGAGCAGGACTGT
CD86-F	CCATCAGCTTGTCTGTTTCATTCC
CD86-R	GCTGTAATCCAAGGAATGTGGTC
CD11c-F	GATGCTCAGAGATACTTCACGGC
CD11c-R	CCACACCATCACTTCTGCGTTC
Arg1-F	TCATCTGGGTGGATGCTCACAC
Arg1-R	GAGAATCCTGGCACATCGGGAA
CD163-F	CCAGAAGGAACTTGTAGCCACAG
CD163-R	CAGGCACCAAGCGTTTTGAGCT
TLR2-F	ATCCTCCAATCAGGCTTCTCT
TLR2-R	GGACAGGTCAAGGCTTTTTTACA
TLR4-F	AGTTGATCTACCAAGCCTTGAGT
TLR4-R	GCTGGTTGTCCCAAATCACTTT
P1-F	CACTGGAGGAACTGGACTCATTTGG
P1-R	GCCCTGTGCTGGTCACCTACG
P2-F	TCCTCTGCCTGGCGAGATGC
P2-R	ACAGCAAAGGAACGGACACACTC
P3-F	GCCGCCTCTGTCTCCCTCTC
P3-R	ACGTCTATCTGTCCGGTGTGTCC
P4-F	GCTCTGCTTCATCCACCTCTTGTC
P4-R	AGTCACCCAGCCACGCTCTAG
Enhancer-F	CTGTCAGGCTTCTGCCTCGT
Enhancer-R	CGAGCGGGAGGCAGAGA
Promoter 1-F	CTGTGGGCTCAGGAGGGC
Promoter 1-R	CACCTGTGGACAGAGGGGC
Promoter 2-F	GGCAGGCATGTTTATTCCCCT
Promoter 2-R	CCCTACAGGAAGAGGCTGGAG
Control-F	GGGCGTGCAGTTATGGCTTA
Control-R	CACCTTGCAGCTCTTACCTGA
NR2F2-F	CTCACCTGGAGCGAGCTGTT
NR2F2-R	AGGGAAGGGAGGCCGAAGCAA
SPI1-F	TGGTGGGTGGACAAGGACAAGG
SPI1-R	TTCGCCGCTGAACTGGTAGGT
ETS1-F	GATAGTTGTGATCGCCTCACC
ETS1-R	GTCCTCTGAGTCGAAGCTGTC
NFATC1-F	TGGAGAAGCAGAGCACGGACAG
NFATC1-R	TGGCGGGAAGGTAGGTGAAACG
TP63-F	GGAAAACAATGCCCAGACTC
TP63-R	GGACTGGTGGACGAGGAG



**Table S4.** The detailed sequence of 3C primers.

<b>3C primers</b>	<b>5'-3'</b>
<b>3C-2-252bp</b> - enhancer	TGAGTAGCTGCTTTCGGTCCG
3C-1-248bp- enhancer	CATGCCCCCAGGTAGAGCT
3C-1-111bp- enhancer	CCGCCTCTCTCTAGCCACC
3C-3-263bp- enhancer	CCAGGCACCTTTCCCTCAC
<b>3C-1-193bp</b> - promoter	GGGCGGAGAAAGAGGGGG
3C-2-168bp- promoter	AGTCTGCAGGCCCCCA
3C-3-223bp- promoter	GCCGAAAGGACACATGGCG
3C-4-302bp- promoter	GGGCGGAGGAGGTGAAGG

**Table S5.** The detailed sequence of sgRNAs used for CRISPR/Cas9-mediated interference of BGN enhancer.

sgRNA	序列
sgP2-2-F	caccgAGAGTGGTTCTCATGTCCGA
sgP2-2-R	aaacTCGGACATGAGAACCACTCTc
sgP3-1-F	caccgGAGAGGGCGGGCGAGCAGGA
sgP3-1-R	aaacTCCTGCTCGCCCGCCCTCTCc
sgP3-2-F	caccgGGGAGGGGACAGCGGGGAGA
sgP3-2-R	aaacTCTCCCGCTGTCCCCTCCCc

**Table S8.** Predicted binding interactions of NR2F2 at the BGN enhancer and promoter according to the JASPAR database.

Name	Score	Relative score	Sequence ID	Start	End	Strand	Predicted sequence
MA1111.2.NR2F2	13.0861810	0.99999999772634	BGNenhancer	1647	1653	-	AAGGTCA
MA1111.2.NR2F2	8.6034810	0.894409179055670	BGNpromoter	1108	1114	-	AGGGTCA
MA1111.2.NR2F2	7.3657150	0.865253363691999	BGNpromoter	868	874	+	AAGGTGA
MA1111.2.NR2F2	7.0944977	0.858864788492441	BGNpromoter	238	244	+	AAGGCCA
MA1111.2.NR2F2	7.0944977	0.858864788492441	BGNpromoter	1406	1412	-	AAGGCCA
MA1111.2.NR2F2	5.3192377	0.817048208591804	BGNpromoter	106	112	-	GGGGTCA
MA1111.2.NR2F2	5.3192377	0.817048208591804	BGNpromoter	114	120	+	GGGGTCA

**Table S9.** Blood biochemical indicators testes of tumor-bearing mice treated with DMSO and CIA1.

Testing items	DMSO	CIA1	Reference range	Units
ALT	41.436 ± 2.489	33.836 ± 15.866	10.06-96.47	U/L
AST	127.397 ± 18.218	112.249 ± 35.953	36.31-235.48	U/L
ALB	32.594 ± 2.068	30.207 ± 4.962	21.22-39.15	g/L
ALP	185.351 ± 22.595	208.753 ± 48.028	22.52-474.35	U/L
γ-GT	0.870 ± 0.267	0.833 ± 0.186	0-7.78	U/L
TBIL	13.457 ± 4.301	13.577 ± 6.132	6.09-53.06	μmol/L
DBIL	3.216 ± 0.444	2.478 ± 0.209	0.45-33.89	μmol/L
BUN	2.436 ± 1.420	2.332 ± 0.074	10.81-34.74	mg/dL
CREA	16.107 ± 5.332	14.335 ± 5.036	10.91-85.09	μmol/L
UA	45.447 ± 0.782	60.445 ± 12.120	44.42-224.77	μmol/L



**Table S10.** Blood routine testes of tumor-bearing mice treated with DMSO and CIA1.

Testing items	DMSO	CIA1	Reference range	Units
WBC	9.8 ± 1.90	7.1 ± 2.86	0.8-10.6	10 <sup>9</sup> /L
Lymph#	6.0 ± 1.83	4.7 ± 2.52	0.6-8.9	10 <sup>9</sup> /L
Mon#	0.4 ± 0.32	0.3 ± 0.16	0.04-1.4	10 <sup>9</sup> /L
Gran#	3.4 ± 0.16	2.1 ± 1.10	0.23-3.6	10 <sup>9</sup> /L
Lymph%	60.23 ± 7.27	64.80 ± 11.99	40-92	%
Mon%	3.93 ± 2.96	5.08 ± 4.06	0.9-18	%
Gran%	35.84 ± 7.42	30.13 ± 12.53	6.5-50	%
RBC	10.53 ± 0.83	10.7 ± 0.80	6.5-11.5	10 <sup>12</sup> /L
HGB	121 ± 14.16	115 ± 4.36	110-165	g/L
HCT	51 ± 3.16	51.8 ± 3.27	35-55	%
MCV	48.5 ± 2.87	48.5 ± 4.67	41-55	fL
MCH	15.4 ± 1.64	15.2 ± 1.78	13-18	pg
MCHC	337 ± 19.54	321 ± 6.86	300-360	g/L
RDW	15.3 ± 2.74	16.3 ± 1.10	12-19	%
PLT	1324 ± 54.74	1171 ± 74.55	400-1600	10 <sup>9</sup> /L
MPV	4.9 ± 0.64	5 ± 0.89	4.0-6.2	fL
PDW	16.2 ± 1.55	16.3 ± 1.01	12.0-17.5	
PCT	0.354 ± 0.25	0.542 ± 0.21	0.100-0.780	%